Torsten Gutmann, Safaa Alkhagani, Niels Rothermel,
Hans-Heinrich Limbach, Hergen Breitzke and Gerd Buntkowsky*

^{31}P-Solid-State NMR Characterization and Catalytic Hydrogenation Tests of Novel heterogenized Iridium-Catalysts

DOI 10.1515/zpch-2016-0837
Received June 28, 2016; accepted October 5, 2016

Abstract: The synthesis of novel robust and stable iridium-based immobilized catalysts on silica-polymer hybrid materials (Si-PB-Ir) is described. These catalysts are characterized by a combination of 1D ^{31}P CP-MAS and 2D ^{31}P-^{1}H HETCOR and J-resolved multinuclear solid state NMR experiments. Different binding situations such as singly and multiply coordinated phosphines are identified. Density functional theory (DFT) calculations are performed to corroborate the interpretation of the experimental NMR data, in order to propose a structural model of the heterogenized catalysts. Finally, the catalytic activity of the Si-PB-Ir catalysts is investigated for the hydrogenation of styrene employing para-enriched hydrogen gas.

Keywords: DFT; heterogeneous catalysis; hydrogenation; iridium; PHIP; solid-state-NMR.

Dedicated to: Prof. Kev Salikhov on the occasion of his 80th birthday.

1 Introduction

Heterogeneous catalysis is used in all sectors of the chemical industry. It combines easy separation of products and reactants with efficient recycling and efficient usage of resources, such as solvents or energy. Despite their importance

***Corresponding author: Gerd Buntkowsky,** Technische Universität Darmstadt, Eduard-Zintl-Institut für Anorganische und Physikalische Chemie, Alarich-Weiss-Str. 8, D-64287 Darmstadt, Germany, e-mail: gerd.buntkowsky@chemie.tu-darmstadt.de
Torsten Gutmann, Safaa Alkhagani, Niels Rothermel and Hergen Breitzke: Technische Universität Darmstadt, Eduard-Zintl-Institut für Anorganische und Physikalische Chemie, Alarich-Weiss-Str. 8, D-64287 Darmstadt, Germany
Hans-Heinrich Limbach: Freie Universität Berlin, FB Biologie, Chemie, Pharmazie, Takustr. 3, D-14195 Berlin, Germany

conventional heterogeneous catalysts, such as for example supported noble metals or oxide catalysts have the disadvantage of low selectivity and specificity. However, these properties are the strength of most homogeneous catalysts. One of the major goals in current catalytic research is the combination of the favorable properties of heterogeneous and homogeneous catalysts by immobilization of a homogeneous catalyst on a solid support material.

Because of this technical importance the development of novel heterogeneous catalysts is a very active ongoing field of research, employing for example functionalized silica hybrid materials [1–11] or polymers as support [12–15]. Furthermore, in the field of metallic nano particles (MNPs) and immobilized MNPs as heterogeneous catalysts many efforts have been made. (see Refs. [16–20] and references therein).

The most common strategy for the immobilization of a homogeneous catalyst is the tethering of the catalyst to the support surface, as for example an oxide, via suitable linkers [21–24]. They were applied for example as efficient systems for hydrosilylation of ketones [25], for hydrogenation or hydroformylation of olefins [26–29], for transfer hydrogenation [30], and for reduction or oxidation of aromatics and alcohols [31–34]. An overview of their application in enantioselective organic synthesis is described in several recent reviews [35–37].

Salient problems of many of these immobilized catalysts are reduced activity and leaching. Both issues result from the replacement of one or several ligands of the homogenous catalyst by linker groups, which effectively replace an optimized ligand with a less-favorable ligand. These issues however limit for example the application of immobilized catalysts in parahydrogen induced polarization (PHIP) experiments in most cases to solid/gas reactions, and only few examples for their use in solid/liquid reactions are known [38–40].

In recent publications we have reported alternative approaches, where immobilized rhodium catalysts were synthesized on support materials, as for example by ligand exchange on cellulose nanoparticles [41], by binding on pydridyl units grafted onto silica nanoparticles [42], or by binding on triphenylphosphine units of [poly (triphenyl phosphine) ethylene (PTPPE)] (4-diphenylphosphine styrene as a monomer) grafted onto silica nanoparticles [43]. In these studies we found that such a strategy combines high catalytic efficacy with stability and excellent leaching properties.

While our previous results focused on rhodium based catalysts, in the present work we present first results on iridium based catalysts. Many Iridium phosphine organometallic complexes are known as efficient homogeneous catalysts. The earliest reports discussing their synthesis, characterization and application in catalysis was the Wilkinson's analogue iridium complex $[IrCl(PPh_3)_3]$ which was reported as square planar [44]. Iridium enables stronger metal-ligand bonds [45].

It can react with hydrogen to produce $[IrH_2Cl(PPh_3)_3]$ but it is not as its analogue Wilkinson's catalyst in dissociation behavior with phosphine ligands. Thus, it is difficult for substrates to have a smooth accessibility [44]. Nevertheless, iridium complexes were synthesized and successfully applied for hydrogenation and asymmetric catalytic reactions [46–48]. Recently, it was also found that some iridium complexes are able to hyperpolarize small molecules via signal amplification by reversible exchange (SABRE) [49, 50].

A main point in the characterization of these solid catalysts is the investigation of their structure and also of the structure of the intermediates of their synthesis. Owing to their highly disordered nature, conventional structure determining techniques like XRD or neutron diffraction are only ill-suited for this. Since solid-state NMR spectroscopy does not depend on high structural order of a system, it has evolved into an indispensable tool for their structural characterization in the last decade [51–59]. An overview and detailed literature references concerning the current state of the art is given in a recent review by some of us [60].

In the present manuscript we report the synthesis and solid-state NMR characterization of novel core-shell NP based catalysts, containing iridium as active metal, and catalytic tests employing para-hydrogen induced polarization (PHIP).

2 Experimental

2.1 Synthesis of the support material

The detailed synthesis of the support material is described in Ref. [43]. Here, only the salient points are summarized. Silica nanoparticles (SiNPs) were activated by keeping overnight at 160°C under vacuum. One gram of freshly activated SiNPs was mixed with 40 mL of THF and 2.41 g of the photoiniferter N,N-(Diethylamino) dithiocarbamoylbenzyl(trimethoxy)silane (PI) (for synthesis of PI see Refs. [61, 62]). The mixture was stirred overnight at room temperature. The product (Si-PI) was obtained after washing with THF and drying under vacuum. By surface-initiated photoiniferter-mediated polymerization (SI-PIMP) the polymer was grown on the surface [63]. For this, 0.5 g of Si-PI was suspended with 40 mL of freshly distilled toluene in a two-neck round-bottom flask and 3.8 g (1.315 mmol) of 4-diphenylphosphine styrene were added. The polymerization was started by irradiating the mixture with UV-light (366 nm). The reaction mixture was kept under constant stirring for 24 h at room temperature. The product Si-PB was washed with toluene in a Soxhlet apparatus. The resulting Si-PB was collected in a flask, dried under vacuum and kept in a glove box. As the polymer-silica hybrid

supporting material Si-PB was already characterized previously by solid-state NMR [43], we reproduce these results in the ESI (Figure S1) to show the quality of the support material.

2.2 Doping with iridium

Two iridium catalysts were prepared employing different synthesis temperatures. 0.1 g of Si-PB were suspended in 50 mL of a mixture of ethanol and 1-propanol and stirred for 15 min at 70°C. 7.34 mg (0.01 mmol) of bis(1,5-cyclooctadiene) diiridium(I) dichloride $[Ir_2Cl_2(COD)_2]$ was added to each of the suspensions which corresponds to an iridium loading of ca 0.2 mmol/g (Ir/Si-PB) assuming a quantitative reaction of the precursor with the supporting material. These suspensions were stirred at 75°C and 85°C, respectively, to later compare structural changes effected by temperature, and left under argon atmosphere and reflux for 90 min. Products were transferred under argon to a Soxhlet apparatus and washed overnight employing ethanol as solvent. The products named as Si-PB-Ir-75 and Si-PB-Ir-85, respectively, dependent on the synthesis temperature, were obtained as light pink powders. They were dried under vacuum and kept in a desiccator.

2.3 Solid-State NMR experiments

All solid state NMR measurements were performed at room temperature under MAS conditions with a Bruker AVANCE II$^+$ spectrometer at 400 MHz proton resonance frequency utilizing a Bruker 4 mm double resonance probe. Ramped CP-MAS sequences were employed to measure ^{31}P spectra at 10 kHz spinning rate [64]. Contact times were set to 3 ms and tppm20 decoupling was used with a 20° phase jump in the course of data acquisition [65]. Spectra were referenced employing H_3PO_4. To record the ^{31}P CP-MAS spectrum of the Si-PB-Ir-85 sample, an additional total suppression of spinning sidebands (TOSS) sequence [66] was employed.

To record the ^{31}P J-resolved solid-state NMR spectrum ^{31}P polarization was produced by means of CP with a contact time of 3 ms followed by a rotor synchronized π-pulse after n rotor periods (n = 1, 2, 3 …) and recording of the spin-echo. The pulse sequence developed by van Rossum et al. [67] was utilized to measure 2D ^{31}P- ^{1}H HETCOR spectra. The contact time was set to 2 ms.

1D-refocused inadequate experiments were conducted by applying ramped-CP-MAS with 2 ms contact time, followed by a rotor synchronized π-τ-$\pi/2$-τ_2-$\pi/2$-τ-π sequence at 10 kHz spinning speed. The delay τ was set as close as possible to

the expected J-coupling, and the delay τ_2 was fixed at 4 μs. Tppm20 decoupling [65] was applied during the π-τ-$\pi/2$-τ_2-$\pi/2$-τ-π sequence as well as in the course of data acquisition.

2.4 Computational details

For DFT calculations we made use of the ORCA [68] program system. All geometry optimizations were performed with Becke's three parameter hybrid functional [69, 70] along with the Lee-Yang-Parr correlation functional (B3LYP), [71] and Pople's double-ζ basis set 6-31G(d,p) [72, 73] combining d- and p-polarization functions. In all calculations the core electrons of iridium were replaced by a relativistic core potential (ECP) developed by the Stuttgart group [74].

Structure models (Figure 3) for three different Ir-complexes (I–III) were created which are based on the structure of Wilkinson's catalyst that was used by Dachs et al. [75] for DFT studies, and on the crystal structure of a related iridium complex published by Laborde et al. (structure 16 in Ref. [76]). For the Wilkinson's type iridium complex I the rhodium was replaced by iridium prior to the geometry optimization. As starting structure for iridium complex II, the bis(triazolylphosphine) ligand system of the iridium complex published by Laborde et al. was replaced by two phosphine ligands. Finally, to imitate the structural environment of the polymeric matrix, the two phosphines in the starting structure of complex II were linked with a pentyl bridge in *para*-position of two neighboring phenyl groups yielding structure III.

2.5 Catalytic activity tests

The catalytic activity was investigated via the hydrogenation reaction of styrene employing para-enriched hydrogen gas, by measurement of ^{1}H NMR spectra. In a typical procedure, 20 mg of the catalyst were dispersed in 2 mL acetone-d_6 in a 5 mL glass vial. The sample was irradiated in an ultrasonic bath for 10 min and heated at 40°C for 15 min. 0.5 mL of this suspension was transferred into a 5 mm screw-capped NMR tube and a mixture of 0.2 mL styrene and 0.3 mL of acetone-d_6 was added. In the first step, the ^{1}H NMR spectrum of the sample was recorded as a background spectrum. Then, the hydrogenation was conducted in the Earth's magnetic field at room temperature or at elevated temperature near the boiling point of the solvent employing a hydrogen gas pressure of ca. 2 bar. The sample was transferred into the strong magnetic field of a seven Tesla superconducting magnet of a Bruker AVANCE III 300 spectrometer after shaking the NMR tube to

initiate the reaction. The waiting time was 1 s to let the sample calm down. The PHIP signal was recorded with a single scan excitation pulse. Finally, several PHIP spectra were recorded until the PHIP antiphase signal disappeared, and the thermally relaxed spectra were measured subsequently.

To ensure that the PHIP signal was generated by the heterogeneous catalyst and not by catalytically active species, which have been leached from the carrier material, a simple "leaching" experiment was performed for all catalysts. In a typical procedure, the reaction mixture was filtered off and the hydrogenation with para-enriched hydrogen was repeated with the filtrate solution.

3 Results and discussion

3.1 Characterization of the support material

In the first step the structures obtained during the synthesis of the silica-polymer hybrid Si-PB material (Scheme 1) were characterized employing a combination of SEM and solid-state NMR techniques. The results of these investigations were already discussed in Ref. [43] and are only briefly summarized here:

The comparison of the SEM pictures (Figure 5a and b in ref. [43]) demonstrated the morphological change of the particles during the grafting process of the polymer. The functionalization of the SiNPs with the photoiniferter N,N-(Diethylamino)dithiocarbamoylbenzyl(trimethoxy)silane (PI) was confirmed by ^{29}Si CP MAS NMR (Figure 1a in Ref. [43]) which showed the appearance of T_n groups in the functionalized Si-PI particles compared to the neat SiNPs. The success of the polymerization of the diphenylphosphine styrene on the Si-PI particles was monitored by ^{13}C CP MAS NMR which showed the disappearance of the C=S signal in the silica-polymer hybrid Si-PB material compared to the Si-PI particles (Figure 2 and Figure 1b in Ref. [43]), indicating the reaction of the monomer with the surface initiator molecules. Furthermore, ^{31}P CP-MAS NMR (ESI Figure S1a) of Si-PB showed one strong signal around −9 ppm. This signal resulted from free phosphine groups of the suggested PTPPE polymer [77]. In the corresponding ^{31}P-^{1}H HETCOR experiment (ESI Figure S1b) it was evident that there is a strong correlation between the aromatic protons centered at 8 ppm as well as of the aliphatic protons at 2 ppm of the polymer backbone and the phosphorous signal at 23 ppm. These observations proved the successful synthesis of the carrier material Si-PB.

In the next step, the binding of iridium to the core-shell-nanoparticles Si-PB was monitored employing different 1D and 2D ^{31}P CP-MAS NMR techniques.

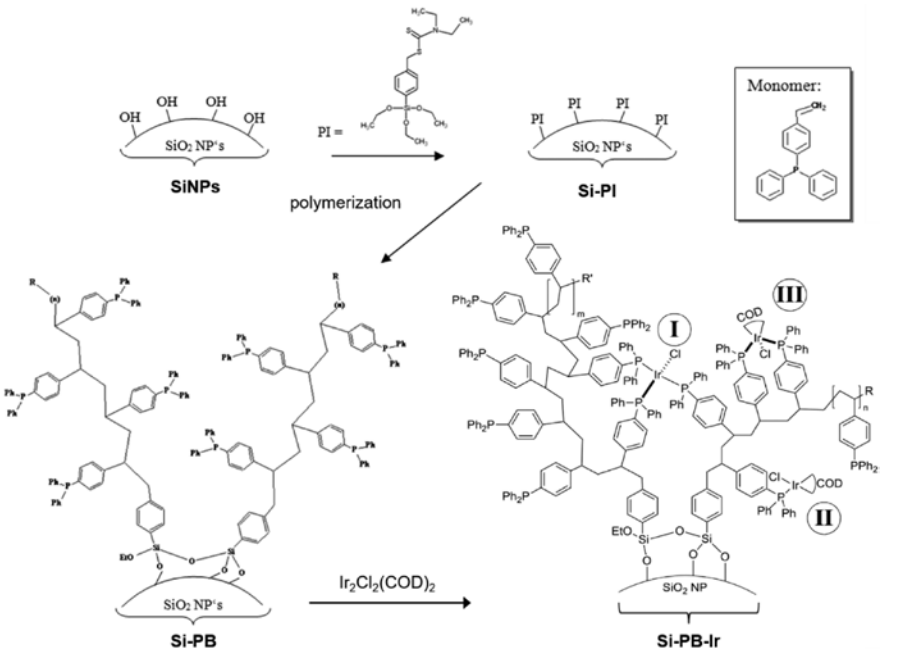

Scheme 1: Reaction scheme of the desired iridium catalyst. First, the silica nanoparticles (SiNPs) were activated. In the second step, the photoinferter (PI) was attached onto the surface of the SiNPs to form Si-PI. In the third step, the polymerization was initiated by the Si-PI to produce polymer brushes (Si-PB). Finally, iridium was embedded between the polymer molecules to obtain the iridium-based catalysts (Si-PB-Ir). Finally, the proposed structure of the mixed bonding situations on Si-PB-Ir catalysts are displayed: (I) Wilkinson's like coordination, (II) singly phosphine coordination, and (III) doubly phosphine coordination.
Note: The reaction scheme and its description was reproduced from Ref. [43].

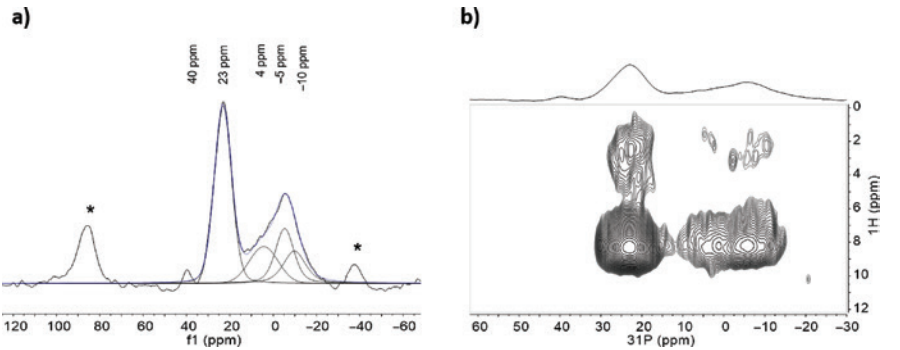

Fig. 1: (a) 31P CP-MAS spectrum of Si-PB-Ir-75, and. (b) 2D 31P-1H HETCOR spectrum with (f1) 1H spectrum and (f2) 31P of Si-PB-Ir-75.
Note: Spectra were recorded at 10 kHz spinning. Spinning side bands are marked with asterisks.

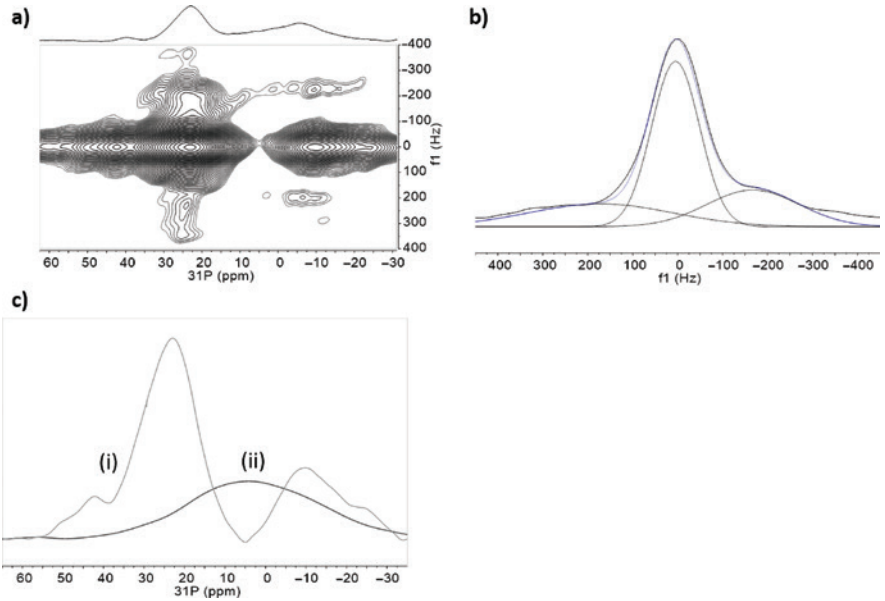

Fig. 2: 2D spectra of Si-PB-Ir-75: (a) ^{31}P *J*-resolved spectrum with (f1) *J*-coupling in Hz and (f2) ^{31}P 1D spectrum. (b) Vertical slice of the ^{31}P *J*-resolved spectrum extracted at 23 ppm. (c) Horizontal slice of the ^{31}P *J*-resolved spectrum extracted at 0 Hz which represents signals showing no J-couplings (i), overlayed with 1D ^{31}P inadequate spectrum which represents signals showing J-couplings (ii).

3.2 ^{31}P CP-MAS measurements of the Si-PB-Ir catalysts

Figure 1a displays the ^{31}P CP-MAS spectrum of the Si-PB-Ir-75 sample. This spectrum exhibits three signals, a small one at 40 ppm and two broad ones at 23 ppm and –4 ppm. Furthermore, the central signal at 23 ppm exhibits strong CSA, visible in the spinning side-bands centered at 85 ppm and –39 ppm. By comparison to our previous paper on the rhodium catalyst [43] the central signal at 23 ppm and the signal at 40 ppm are attributed to bound phosphine groups and oxidized phosphine groups at the polymer, respectively. The assignment of the signal at 23 ppm to bound phosphine species is in excellent agreement with the ^{31}P CP-MAS spectrum for the Wilkinson's analog iridium complex $IrCl(PPh_3)_3$ (ESI Figure S3) which displays a group of resolved signals centered at ca. 23 ppm with corresponding spinning sidebands centered at 85 ppm and –39 ppm. This observation is a first indication that the new immobilized Si-PB-Ir-75 catalyst contains binding geometries on Ir which are comparable to the neat $IrCl(PPh_3)_3$ catalyst.

The broad asymmetric high-field line with a maximum intensity at –4 ppm can be deconvoluted into three signals located at –10 ppm, –5 ppm and +4 ppm. While the latter two signals indicate the presence of other phosphine species coordinating iridium, the signal at –10 ppm assigns to unbound phosphines when compared with the neat Si-PB support material (–9 ppm) (ESI Figure S1a).

Although iridium has two low-gamma spin 3/2 quadrupolar isotopes (^{191}Ir and ^{193}Ir) with natural abundances of 37% and 63%, there are no resolved ^{31}P- $^{191/193}$Ir J-couplings visible in the ^{31}P CP-MAS spectra, in contrast to the rhodium catalysts studied previously by us [43]. Such observation is not very surprising, since both of these nuclei possess very large quadrupolar moments, which lead to fast quadrupolar relaxation i.e. fast spin flipping. This will lead to "self-decoupling" as mentioned by Wasylishen and co-workers for square planar iridium phosphine complexes [78].

For comparison, the spectrum of Si-PB-Ir-85 is shown in ESI Figure S4a. While the central line is again observed at ca. 23 ppm, the line at 40 ppm is slightly high-field shifted to 38 ppm. Additionally, signals between –10 and +10 ppm became clearly visible as shoulders in the line-shape, which indicate some structural differences with respect to the Si-PB-Ir-75 sample. Performing a line-shape analysis of these shoulders reveals two signals at 10 ppm and 3 ppm, which is again a strong hint for the presence of a second type of phosphine-iridium binding situation. Finally, a signal at –8 ppm appeared, which most probably assigns non-coordinating phosphine groups in the polymer chains.

3.3 2D-NMR measurements of the Si-PB-Ir catalysts

To shed more light on the binding situation of the phosphines, and in order to perform a detailed interpretation of the obtained chemical shifts in the 1D ^{31}P CP-MAS spectra, additional 2D spectra were recorded. Figure 1b displays the results of the ^{31}P-^{1}H heteronuclear correlation measurements and Figure 2a the 2D *J*-resolved ^{31}P-^{31}P homonuclear correlation spectra for Si-PB-Ir-75.

From the ^{31}P-^{1}H HETCOR experiment (Figure 1b) it is evident that there is a strong correlation between the aromatic protons centered at 8 ppm and the phosphorous signal at 23 ppm. A second weaker cross-peak is found between ^{31}P at 23 ppm and the aliphatic backbone protons at 2 ppm. These cross-peaks clearly validate the assignment that these phosphorous signals are from the phosphine groups of the polymer. The broad high field signal at –4 ppm displays a strong interaction with the aromatic ^{1}H and a weak one with the aliphatic protons. This observation corroborates that the aromatic protons are closer to the phosphorous than the aliphatic protons. Similar results were obtained in our

previous study on Si-PB-Rh (see ESI Figure S1a) and for the Si-PB-Ir-85 sample (see ESI Figure S4b).

While the 2D *J*-resolved ^{31}P-^{31}P homonuclear correlation spectrum of Si-PB-Ir-75 (Figure 2a) does not show resolved ^{31}P-^{31}P-couplings for the signal at 23 ppm there is a substantial broadening in the indirect dimension for this sample which indicates the presence of homonuclear scalar couplings. The line-shape analysis of the vertical slice extracted at 23 ppm (Figure 2b) suggests the presence of two different types of phosphorous. The first type does not exhibit any resolved ^{31}P-^{31}P J-coupling, which most probably refers to phosphines in a *cis*-configuration or to oxidized phosphines on the polymer surface. The second type of phosphorous exhibits a coupling of ca. 400 Hz, which is characteristic for phosphines in *trans*-configuration (comparable with Wilkinson's type catalyst [79, 80]). This observation is underlined by comparison of the horizontal slice of the ^{31}P *J*-resolved spectrum extracted at 0 Hz, showing a maximum around 23 ppm [Figure 2c (i)], with the 1D ^{31}P inadequate spectrum containing only a small shoulder around 23 ppm [Figure 2c (ii)]. All these observations strongly indicate multiple coordination of a substantial number of phosphines to the iridium.

Finally, the existence of scalar couplings for the signals between 0 and 10 ppm is indicated by the ^{31}P INADEQUATE, which shows a signal in this region. [Figure 2c (ii)]. This corroborates our previous hypothesis, that signal components in the range of 0–10 ppm assign a second type of phosphine-iridium binding situations and further lead to the assumption of doubly coordinating phosphine groups.

3.4 DFT calculations

To corroborate the interpretation of the NMR spectra in terms of binding situations of phosphines in our Si-PB-Ir catalysts, probable iridium model complexes (Figure 3a) were designed, and their binding geometries were optimized based on density functional theory (DFT).

As most experimental studies of phosphine coordinated iridium complexes referred to four-fold coordinated iridium in a square planar binding geometry, as first example the Wilkinson's analog complex $IrCl(PPh_3)_3$ (I) was investigated. In a further step complexes were modeled based on the iridium complex published by Laborde et al. [76] which contains a cyclooctadiene (COD) ligand. Since the iridium precursor, employed for our synthesis of the Si-PB-Ir catalysts, also contained such COD ligands, it is assumed that COD is also present in the immobilized catalyst. Thus, two model systems based on the iridium complex by Laborde

a)

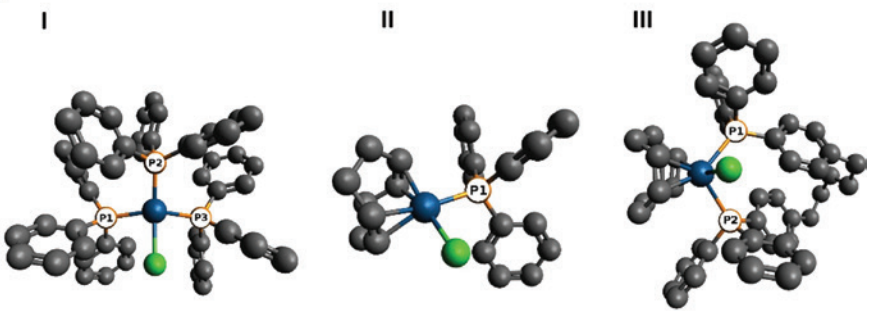

b)

I		II		III	
bond	lenght / Å	bond	lenght / Å	bond	lenght / Å
P1-Ir	2.38	P1-Ir	2.38	P1-Ir	2.54
P2-Ir	2.27			P2-Ir	2.56
P3-Ir	2.36				

Fig. 3: (a) Optimized geometries of iridium model complexes: Wilkinson's type Ir-complex (I), singly phosphine coordinated Ir-complex containing a COD ligand (II), and doubly phosphine coordinated Ir-complex containing a COD ligand (III). (b) Bond lengths for iridium phosphorous bonds in complexes I-III derived after structure optimization at the B3LYP/6-31G(d,p) level of theory.

were studied. For the first case, where the two phosphine groups were not connected via an alkyl bridge the geometry optimization converged into structure II, by releasing one phosphine group. For the second case, where the phosphine groups are bridged, structure III was stabilized.

After geometry optimization of the complexes, the Ir-P bond lengths were analyzed (Figure 3b) since they indirectly give information on the electron density at the phosphorous atoms which correlates with the chemical shielding. While for complexes I and II, bond lengths of ca. 2.38 Å were found, for complex III bond lengths of ca. 2.55 Å were obtained.

These values clearly show, that in case of complexes I and II the Ir-P bond strength is larger than in complex III, which is aligned with the metal to ligand π-backbond from the Ir to the π* orbital of the phosphorous. In case of complexes I and II the π-backbond seems weaker than for complex III which is reflected in the shorter Ir-P bond length for complex I and II. This however means that for complex III a higher electron density at the phosphorous is assumed which yield a higher shielding compared to complex I and II.

With these results a distinct interpretation of the observed chemical shifts in the NMR spectra of Si-PB-Ir becomes feasible. The main component at 23 ppm

most probably assigns to coordinated iridium-phosphine species similar to the binding situation in Wilkinson's catalyst referring to model I, which is formed by multiple coordination of phosphines from different polymer brushes. Furthermore, singly coordinated phosphines referring to model II are feasible.

The signal components between 0 and 10 ppm assign to phosphine groups in a coordination referring to model III, where, most probably, two phosphine groups in one polymer chain are coordinating the Ir center.

3.5 Binding model

Putting all experimental and theoretical results together we come to the following picture, which is schematically shown in Scheme 1. In contrast to the rhodium catalyst studied previously by us [43], the situation for the iridium is more complex. There is a distribution of iridium sites with different phosphorus coordination of the metal center. The singly phosphine coordination is dominating [Scheme 1 (II)], however also triple coordination as in Wilkinson's type catalysts [Scheme 1 (I)] is feasible, which most probably occurs when iridium is coordinated by phosphines from different polymer brushes.

Finally, the signals between 0 and 10 ppm obtained in the ^{31}P CP-MAS spectrum (Figure 1a) combined with the DFT calculations on model III (Figure 3) proposed an additional type of doubly coordination of phosphines where two phosphines are bridged via the polymer chain [Scheme 1 (III)]. Since calculations were only performed for a small model system containing a pentyl bridge, the polymer brush is not fully described. Thus, larger P-Ir-P bond angles compared to model III are in principle possible which would explain the obtained J-coupling for the signals between 0 and 10 ppm.

3.6 Evaluation of the catalytic efficacy

The hydrogenation of styrene as a model reaction employing *para*-H_2, which is a standard reaction for the evaluation of PHIP-catalysts, was employed for the assessment of the catalytic efficacy of the new catalysts.

Figure 4 displays the results of the two iridium catalysts. The left panel shows the results obtained with Si-PB-Ir-75. The first three spectra display the background (a), the hydrogenation at room temperature (b) and the thermally relaxed spectrum (c). The next two spectra are measured after hydrogenation at elevated temperature close to the boiling point of the solvent (d), and the resulting thermally relaxed spectrum (e). The hydrogenation product is clearly visible in the

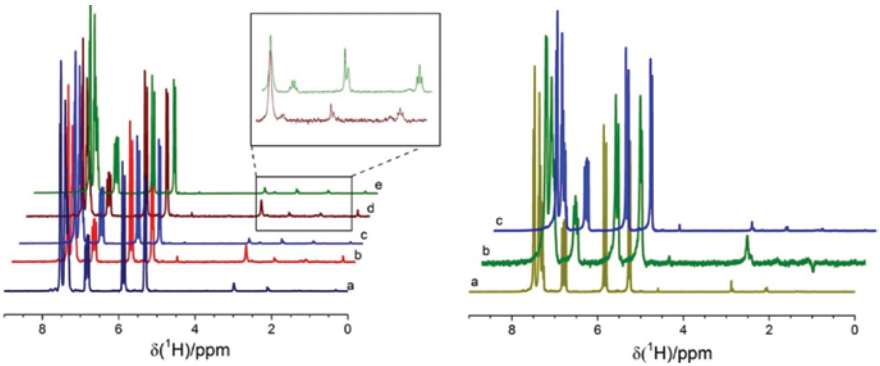

Fig. 4: ^{1}H spectra of styrene hydrogenation employing *para*-enriched H_2 under ALTADENA [81] conditions. Left panel: Si-PB-Ir-75 (a) background; (b) hydrogenation; (c) thermal relaxed of b spectrum, (d) hydrogenation at elevated temperature, (e) thermal relaxed spectrum of d. Right panel: Si-PB-Ir-85 (a) Background spectrum; (b) Hyperpolarized spectrum at elevated temperature; (c) thermal polarized spectrum (relaxed) of b.

spectra, however, no PHIP pattern was detected. Thus, the hydrogenation reaction indicates that the active sites are able to combine both with hydrogen and styrene using the catalyst Si-PB-Ir-75 but are not able to maintain the hyperpolarized state during the hyperpolarization.

The situation changes for the sample Si-PB-Ir-85. Here a distinct PHIP pattern is observable. The calculated enhancement factor is 5 for the methylene group at 2.8 ppm and 3 for the methyl group at 1.3 ppm. The filtrate of the hydrogenation mixture was tested to discover whether any catalytic activity could be detected for any leached species but nothing was observed [82]. This is a direct indication that the iridium example is a robust and stable catalyst and can be used to produce a hyperpolarized NMR signal as well as in the rhodium example Si-PB-Rh reported recently [43].

Although it is not finally clear what causes the difference between the two new iridium catalysts Si-PB-Ir-75, Si-PB-Ir-85 and the previously studied rhodium sample at least a tentative interpretation will be attempted. Iridium has a larger coordination sphere than the previously studied rhodium. This may cause problems in the accessibility of the iridium center, which are more pronounced in the low-temperature sample than in the high-temperature sample, and the better efficacy results from the differences in the coordination of the iridium in the two samples. Thus, the reaction rates would be mainly diffusion controlled.

4 Summary and conclusions

The successful synthesis of novel immobilized iridium catalysts on silica-polymer hybrid materials (Si-PB-Ir) was described. These catalysts contain different binding situations of phosphines as evidenced by a combination of 1D ^{31}P CP-MAS, and 2D ^{31}P-^{1}H HETCOR and J-resolved multinuclear solid state NMR experiments. In combination with these experimental data, density functional theory (DFT) calculations on model complexes derived from an iridium analogue Wilkinson's catalyst and a COD containing iridium complex were performed, to propose a structural model of the heterogenized catalysts. This structure contains singly and multiply coordinated phosphine groups in different binding geometries. Catalytic test experiments of the Si-PB-Ir catalysts revealed significant activity of the catalysts in the hydrogenation of styrene employing para-enriched hydrogen gas. No significant leaching of catalytically active species was obtained. This shows that the novel Si-PB-Ir catalysts may join the rhodium catalyst (Si-PB-Rh) as a group of heterogeneous, robust and stable catalysts.

Acknowledgments: Financial support by the Deutsche Forschungsgemeinschaft under contract BU-911-22-1 is gratefully acknowledged. We thank Ömer Faruk Delibalta for the help in the synthesis of the materials.

References

1. A. Corma, H. Garcia, Adv. Synth. Catal. **348** (2006) 1391.
2. A. Grünberg, H. Breitzke, G. Buntkowsky, Solid state NMR of immobilized catalysts and nanocatalysts **43** (2012) 289.
3. F. Hoffmann, M. Cornelius, J. Morell, M. Froeba, Angew. Chem.- Int. Ed. **45** (2006) 3216.
4. A. Sayari, S. Hamoudi, Chem. Mater. **13** (2001) 3151.
5. A. Stein, Adv. Mater. **15** (2003) 763.
6. A. Vinu, K. Z. Hossain, K. Ariga, J. Nanosci. Nanotechnol. **5** (2005) 347.
7. J. Y. Ying, C. P. Mehnert, M. S. Wong, Angew. Chem.- Int. Ed. **38** (1999) 56.
8. X. S. Zhao, X. Y. Bao, W. Guo, F. Y. Lee, Mater. Today **9** (2006) 32.
9. H. I. Lee, J. H. Kim, G. D. Stucky, Y. F. Shi, C. Pak, J. M. Kim, J. Mater. Chem. **20** (2010) 8483.
10. A. Taguchi, F. Schueth, Microporous Mesoporous Mater. **77** (2005) 1.
11. X. S. Zhao, G. Q. M. Lu, G. J. Millar, Ind. Eng. Chem. Res. **35** (1996) 2075.
12. M. Benaglia, A. Puglisi, F. Cozzi, Chem. Rev. **103** (2003) 3401.
13. D. Brunel, N. Bellocq, P. Sutra, A. Cauvel, M. Laspéras, P. Moreau, F. Di Renzo, A. Galarneau, F. Fajula, Coord. Chem. Rev. **178** (1998) 1085.
14. E. Lindner, T. Schneller, F. Auer, H. A. Mayer, Angew. Chem.- Int. Ed. **38 (**1999) 2154.
15. J. Lu, P. H. Toy, Chem. Rev. **109** (2009) 815.
16. D. Astruc, Nanoparticles and Catalysis, Wiley-VCH, Weinheim (2008).

17. P. Lara, K. Philippot, B. Chaudret, Chem. Cat. Chem. **5** (2013) 28.
18. A. Roucoux, J. Schulz, H. Patin, Chem. Rev. **102** (2002) 3757.
19. T. Gutmann, I. del Rosal, B. Chaudret, R. Poteau, H.-H. Limbach, G. Buntkowsky, Chem. Phys. Chem. **14** (2013) 3026.
20. N. F. Zheng, G. D. Stucky, *J. Am. Chem. Soc.* **128** (2006) 14278.
21. C. Merckle, S. Haubrich, J. Blümel, J. Organomet. Chem. **627** (2001) 44.
22. C. Merckle, J. Blümel, Top. Catal. **34** (2005) 5.
23. B. Beele, J. Guenther, M. Perera, M. Stach, T. Oeser, J. Blümel, New J. Chem. **34** (2010) 2729.
24. J. Guenther, J. Reibenspies, J. Bluemel, Adv. Synth. Catal. **353** (2011) 443.
25. G. Hamasaka, S. Kawamorita, A. Ochida, R. Akiyama, K. Hara, A. Fukuoka, K. Asakura, W. J. Chun, H. Ohmiya, M. Sawamura, Organometallics **27** (2008) 6495.
26. T. Joseph, S. S. Deshpande, S. B. Halligudi, A. Vinu, S. Ernst, M. Hartmann, J. Mol. Catal. A **206** (2003), 13.
27. L. Huang, J. C. Wu, S. Kawi, React. Kinet. Catal. Lett. **82** (2004) 65.
28. V. Dufaud, F. Beauchesne, L. Bonneviot, Angew. Chem.- Int. Ed. **44** (2005) 3475.
29. A. Crosman, W. E. Hoelderich, J. Catal. **232** (2005) 43.
30. K. Bogár, P. Krumlinde, Z. Bacsik, N. Hedin, J.-E. Backvall, Eur. J. Org. Chem. (2011) 4409.
31. O. A. Anunziata, A. R. Beltramone, M. L. Martinez, L. L. Belon, J. Colloid Interface Sci. **315** (2007) 184.
32. J. Evans, A. B. Zaki, M. Y. El-Sheikh, S. A. El-Safty, J. Phys. Chem. B **104** (2000) 10271.
33. W.-H. Cheung, W.-Y. Yu, W.-P. Yip, N.-Y. Zhu, C.-M. Che, J. Org. Chem. **67** (2002) 7716.
34. S. Shylesh, A. P. Singh, J. Catal. **228** (2004) 333.
35. J. M. Fraile, J. I. Garcia, J. A. Mayoral, Chem. Rev. **109** (2009) 360.
36. M. Heitbaum, F. Glorius, I. Escher, Angew. Chem.- Int. Ed. **45** (2006) 4732.
37. C. Jimeno, S. Sayalero, M. A. Pericas, in: Heterogenized Homogeneous Catalysts for Fine Chemicals Production: Materials and Processes, (2010), vol. 33, p. 123.
38. I. V. Koptyug, K. V. Kovtunov, S. R. Burt, M. S. Anwar, C. Hilty, S.-I. Han, A. Pines, R. Z. Sagdeev, J. Am. Chem. Soc. **129** (2007) 5580.
39. A. M. Balu, S. B. Duckett, R. Luque, Dalton Trans. (2009) 5074.
40. I. V. Koptyug, V. V. Zhivonitko, K. V. Kovtunov, Chem. Phys. Chem. **11** (2010) 3086.
41. T. Gutmann, J. Liu, N. Rothermel, Y. Xu, E. Jaumann, M. Werner, H. Breitzke, S. T. Sigurdsson, G. Buntkowsky, Chem. -Eur. J. **21** (2015) 3798.
42. M. Srour, S. Hadjiali, G. Sauer, K. Brunnengräber, H. Breitzke, Y. Xu, H. Weidler, H.-H. Limbach, T. Gutmann, G. Buntkowsky, Chem. Cat. Chem. (2016) DOI: 10.1002/cctc.201600882.
43. S. Abdulhussain, H. Breitzke, T. Ratajczyk, A. Grünberg, M. Srour, D. Arnaut, H. Weidler, U. Kunz, H. J. Kleebe, U. Bommerich, Chem. -A Eur. J. **20** (2014) 1159.
44. R. H. Crabtree, Plati. Met. Rev. **22** (1978) 126.
45. R. H. Crabtree, in: The Handbook of Homogeneous Hydrogenation, Wiley-VCH Verlag GmbH (2008), P. 31.
46. T. L. Church, P. G. Andersson, Coord. Chem. Rev. **252** (2008) 513.
47. L. Vaska, J. W. DiLuzio, J. Am. Chem. Soc. **83** (1961) 2784.
48. R. H. Crabtree, H. Felkin, G. E. Morris, J. Organomet. Chem. **141** (1977) 205.
49. B. J. A. van Weerdenburg, S. Gloggler, N. Eshuis, A. H. J. Engwerda, J. M. M. Smits, R. de Gelder, S. Appelt, S. S. Wymenga, M. Tessari, M. C. Feiters, B. Blumich, F. P. J. T. Rutjes, Chem. Comm. **49** (2013) 7388.

50. M. Fekete, O. Bayfield, S. B. Duckett, S. Hart, R. E. Mewis, N. Pridmore, P. J. Rayner, A. Whitwood, Inorg. Chem. **52** (2013) 13453.
51. J. Bluemel, Coord. Chem. Rev. **252** (2008) 2410.
52. M. Lelli, D. Gajan, A. Lesage, M. A. Caporini, V. Vitzthum, P. Mieville, F. Heroguel, F. Rascon, A. Roussey, C. Thieuleux, M. Boualleg, L. Veyre, G. Bodenhausen, C. Coperet, L. Emsley, J. Am. Chem. Soc. **133** (2011) 2104.
53. A. Lesage, M. Lelli, D. Gajan, M. A. Caporini, V. Vitzthum, P. Mieville, J. Alauzun, A. Roussey, C. Thieuleux, A. Mehdi, G. Bodenhausen, C. Coperet, L. Emsley, J. Am. Chem. Soc. **132** (2010) 15459.
54. K. Mao, J. W. Wiench, V. S. Y. Lin, M. Pruski, J. Magn. Reson. **196** (2009) 92.
55. Adamczyk, Y. Xu, B. Walaszek, F. Roelofs, T. Pery, K. Pelzer, K. Philippot, B. Chaudret, H. H. Limbach, H. Breitzke, G. Buntkowsky, Top. Catal. **48** (2008) 75.
56. J. L. Rapp, Y. Huang, M. Natella, Y. Cai, V. S. Y. Lin, M. Pruski, Solid State Nucl. Magn. Reson. **35** (2009) 82.
57. J. W. Wiench, C. Michon, A. Ellern, P. Hazendonk, A. Iuga, R. J. Angelici, M. Pruski, J. Am. Chem. Soc. **131** (2009) 11801.
58. A. Grünberg, X. Yeping, H. Breitzke, G. Buntkowsky, Chem. – Eur. J. **16** (2010) 6993.
59. A. Gruenberg, T. Gutmann, N. Rothermel, Y. Xu, H. Breitzke, G. Buntkowsky, Z. Phys. Chem. **227** (2013) 901.
60. T. Gutmann, A. Grünberg, N. Rothermel, M. Werner, M. Srour, S. Abdulhussain, S. L. Tan, Y. P. Xu, H. Breitzke, G. Buntkowsky, Solid State Nucl. Magn. Reson. **55–56** (2013) 1.
61. T. Otsu, M. Yoshida, Makromol. Chem.-Rapid Commun. **3** (1982) 127.
62. B. de Boer, H. K. Simon, M. P. L. Werts, E. W. van der Vegte, G. Hadziioannou, Macromolecules **33** (2000) 349.
63. B. de Boer, H. K. Simon, M. P. L. Werts, E. W. van der Vegte, G. Hadziioannou, Macromolecules **33** (1999) 349.
64. A. E. Bennett, C. M. Rienstra, M. Auger, K. V. Lakshmi, R. G. Griffin, J. Chem. Phys. **103** (1995) 6951.
65. D. G. Cory, W. M. Ritchey, J. Magn. Reson. **80** (1988) 128.
66. W. T. Dixon, J. Schaefer, M. D. Sefcik, E. O. Stejskal, R. A. McKay, J. Magn. Reson. (1969), **49** (1982) 341.
67. B. J. van Rossum, H. Förster, H. J. M. de Groot, J. Magn. Reson. **124** (1997) 516.
68. F. Neese, Wiley Interdiscip. Rev. Comput. Mol. Sci. **2** (2012) 73.
69. A. D. Becke, J. Chem. Phys. **98** (1993) 1372.
70. A. D. Becke, J. Chem. Phys. **98** (1993) 5648.
71. C. T. Lee, W. T. Yang, R. G. Parr, Phys. Rev. B **37** (1988) 785.
72. J. D. Dill, J. A. Pople, J. Chem. Phys. **62** (1975) 2921.
73. W. J. Hehre, R. Ditchfield, J. A. Pople, J. Chem. Phys. **56** (1972) 2257.
74. D. Figgen, K. A. Peterson, M. Dolg, H. Stoll, J. Chem. Phys. **130** (2009) 164108.
75. A. Dachs, S. Osuna, A. Roglans, M. Solà, Organometallics **29** (2010) 562.
76. C. Laborde, M.-M. Wei, A. van der Lee, E. Deydier, J.-C. Daran, J.-N. Volle, R. Poli, J.-L. Pirat, E. Manoury, D. Virieux, Dalton Trans. **44** (2015) 12539.
77. C.-W. Tsang, B. Baharloo, D. Riendl, M. Yam, D. P. Gates, Angew. Chem.- Int. Ed. **43** (2004) 5682.
78. G. Wu, R. E. Wasylishen, Inorg. Chem. **33** (1994) 2774.
79. A. Gruenberg, Y. P. Xu, H. Breitzke, G. Buntkowsky, Chemistry-a European Journal **16** (2010) 6993.

80. G. Wu, R. E. Wasylishen, Inorg. Chem. **31** (1992) 145.
81. M. G. Pravica, D. P. Weitekamp, Chem. Phys. Lett. **145** (1988) 255.
82. T. Gutmann, T. Ratajczyk, Y. Xu, H. Breitzke, A. Grünberg, S. Dillenberger, U. Bommerich, T. Trantzschel, J. Bernarding, G. Buntkowsky, Solid State Nucl. Magn. Reson. **38** (2010) 90.

Supplemental Material: The online version of this article (DOI: 10.1515/zpch-2016-0837) offers supplementary material, available to authorized users.